Two-Section Reactor Model for Autothermal Reforming of Methane to Synthesis Gas

P. Maarten Biesheuvel and Gert Jan Kramer
Shell Global Solutions International B.V., Badhuisweg 3, 1031 CM, Amsterdam, The Netherlands
and
HydrogenSource LLC, South Windsor, CT 06074

A 1-D stationary reactor model describes the catalytic conversion of a gaseous hydrocarbon fuel with air and steam to synthesis gas by autothermal reforming and catalytic partial oxidation. The model defines two subsequent sections in the reactor: an upstream oxidation section and a downstream reforming section. In the oxidation section, all of the oxygen is converted, with partial conversion of the fuel. An empirical fuel utilization ratio is used to quantify which part of the fuel is converted in the oxidation section as a function of the relative flows of air and steam. In the oxidation section, the gas temperature rapidly increases toward the top temperature at the intersection with the reforming section. In this section the temperature decreases while the fuel is further converted with water and CO_2 as oxidant. For methane as fuel, simulation results are compared with experiments. For multicomponent fuels such as natural gas and naphtha, application of the two-section model is described.

Introduction

Hydrogen is manufactured industrially from hydrocarbon fuels either by steam reforming or by gasification (Rostrup-Nielsen, 1993). In steam reforming, the fuel (in most cases, natural gas) reacts with steam toward synthesis gas over a Ni-based heterogeneous catalyst. Due to the endothermicity of the steam reforming reaction, heat must be supplied to the reactor through the reactor tube walls. Gasification is an autothermal process in which the fuel is mixed with pure oxygen and noncatalytically converted to synthesis gas. An example of its industrial use is the Shell Gasication Process (Elvers et al., 1989).

The recent surge in demand for on-spot, small-scale, cheap and simple hydrogen production technologies based on hydrocarbon fuels is driven by the interest in fuel cells for electricity generation (Docter and Lamm, 1999; Ahmed and Krumpelt, 2001; Moon et al., 2001). Light hydrocarbon fuels, such as natural gas, are envisioned for stationary applications, such as at the scale of a single household (1–5 kWe, kW electricity), while liquid fuels (gasoline, naphtha) have

potential for automotive applications (25–75 kWe; Service, 1999). To obtain a gas mixture that can be fed to a fuel cell, the hydrocarbon fuel is first converted to synthesis gas in a reformer. When a proton exchange membrane (PEM) fuel cell is used, the synthesis gas must be further processed, first in a water-gas-shift reactor, where CO is converted to CO_2 and additional hydrogen is obtained, after which remaining traces of CO are removed (such as by selective oxidation) before the mixture is finally fed to the anode side of the fuel cell.

For these applications, down-scaled versions of the gasification and steam reforming processes are impractical. First of all, downscaling is not very well possible (especially for gasification) and, otherwise, the resulting processes are too bulky, expensive, and difficult to operate. However, an air-based, autothermal catalytic fixed-bed technology, in which the hydrocarbon fuel is mixed with air and steam, may result in a small reformer that is safe and easy to operate and automate. Two technologies are available, derived from their industrial analogues. Autothermal reforming (ATR), based on mixing air in with the steam/fuel mixture, is an autothermal adaptation of steam reforming. In the gasification process, it is possible to replace the oxygen with air and use a catalyst

---

instead of an underoxidized burner; this is catalytic partial oxidation (CPO). CPO has—within Shell—originally been developed as a catalytic alternative for the industrial SGP process. Originally intended for operation with pure oxygen, it has been modified for use with air and steam to suit the needs of fuel processing for fuel cells.

While the two technologies have a distinctly different origin, we are of the opinion that the two technologies have all but merged, although CPO typically operates at low to zero steam-to-carbon ratios (such as $S/C < 1$), while ATR operates at a higher steam load ($S/C > 1$). In ATR and CPO several similar catalyst systems have been used and tested, such as those based on supported precious metals. In both processes the aim is to achieve the thermodynamic equilibrium composition, which is determined by feed conditions (composition, temperature), pressure, and heat loss. These conditions are optimized to obtain a maximum *syngas yield* in hydrogen and carbon monoxide (in the relevant yield figure, CO is added to H_2, because of its conversion in the subsequent water-gas-shift reactor), as well as to minimize slip of hydrocarbons (especially methane levels can be significant at thermodynamic equilibrium, dependent on exit temperature and amount of steam).

Comparing CPO with ATR, in CPO temperatures in the catalyst bed tend to be higher and syngas yield somewhat lower. However, premixing and preheating is more straightforward (certainly for $S/C = 0$) and reaction rates tend to be higher (higher space velocity possible). In any case, the choice for the optimal air/fuel and steam/fuel ratio, as well as inlet temperature and operating pressure, must be made at the level of the entire fuel processor system.

It must be stressed that both in CPO and ATR the practical objective is to bring the mixture to thermodynamic equilibrium. While there is no *a priori* reason why a catalytic process could not be more selective towards syngas than what is dictated by thermodynamics, the fact that CO and hydrogen are so much more reactive with oxygen than the feed hydrocarbon molecules makes this goal elusive. This reactivity bias will in fact cause an "overshoot" of the reaction: excess amounts of CO_2 and water are produced at the "top" of the
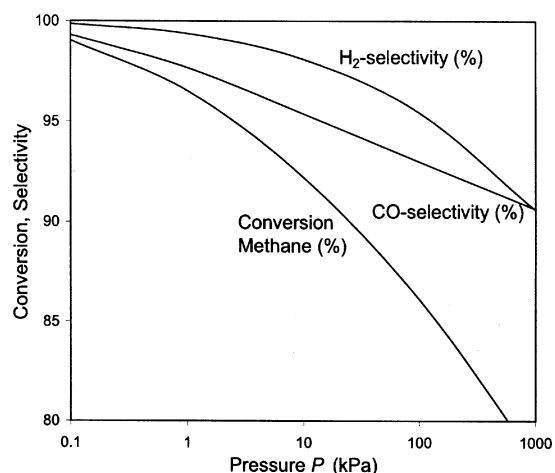
Figure 2. **Thermodynamic equilibrium in adiabatic operation of air-based CPO of methane (no steam, $O_2/C = 0.5$, air: 21 mol% O_2, 79% N_2), $T_{inlet} = 300°C$.**

Methane conversion and selectivities to CO and H_2 as function of pressure.

reactor (see Figure 1), after which thermodynamic equilibrium is approached via reforming reactions. Thus, if thermodynamic equilibrium is not reached, there is both an excess amount of CO_2 and water, as well as an unnecessary slip of methane and higher hydrocarbons, both leading to a suboptimal syngas yield.

A second aspect of thermodynamic equilibrium is that for operation at low air and steam flows (relative to the fuel), such as done almost by definition in studies of "pure" CPO of methane (studies in which the O_2/CH_4 ratio is set to 0.5 and no steam is added, based on $CH_4 + 0.5\ O_2 \rightarrow CO + 2H_2$), CH_4-conversion and CO- and H_2-selectivities are clearly below 100% unless operation is at a very high (inlet) temperature or a very low pressure (Dissanayake et al., 1991; Wang and Ruckenstein, 1999). Results of thermodynamic calculations are shown in Figure 2 for adiabatic CPO of methane without steam and with air ($O_2/CH_4 = 0.5$). In this case, only by decreasing the pressure to very low values is it possible to obtain full methane conversion and 100% selectivity toward H_2 and CO. Thus, incomplete methane conversion and nonselective behavior at practical conditions (T, P) is not necessarily due to a catalyst with poor selectivity/activity, but, in many cases, a direct consequence of the thermodynamic equilibrium (Prettre et al., 1946; Chang and Heinemann, 1993; Bodke et al., 1998). In practice this is well-known and to optimize syngas yield and keep methane slip below a certain threshold, more air (and/or water) are added than the "pure CPO" reaction suggests (for example, Kramer et al., 2001).

Thermodynamic equilibrium models required for the above calculations (both for CPO and ATR) are readily available or are rather easily set up, such as based on (part of) the equations used in this article (Docter and Lamm, 1999). However, for reactor design and catalyst development, nonequilibrium reactor modeling is required.

This article will focus on the development of a reactor model that describes the approach to thermodynamic equilib-
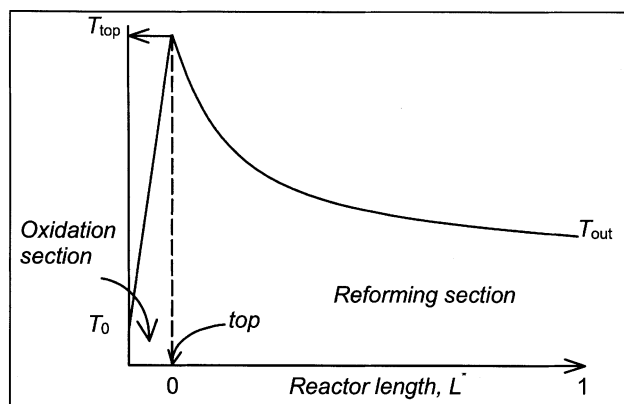

Figure 1. **Gas-phase temperature in CPO/ATR of methane.**

The measured catalyst temperature at the upstream side is assumed equal to the gas phase temperature at the intersection of the oxidation and reforming section (0, "top").

rium, thus reflecting the situation in practical reactors. Obviously, it is required that the model is thermodynamically consistent at each reactor coordinate (at each location). By this, we mean that the equations that are used at each location to describe the conversion of the off-equilibrium gas mixture only contain local parameters (local temperature, gas composition), but correctly predict the thermodynamic equilibrium composition and temperature when given enough residence time or space. To be practical, the model must contain a limited number of fit parameters (reaction orders, activation energy, kinetic constants, and so on). Furthermore, the high upstream temperature (top temperature) that is observed in CPO/ATR (Prettre et al., 1946; Papp et al., 1996; Heitnes Hofstad et al., 1997; Wang and Ruckenstein, 1999) must be an integral part of the model. Finally, atomic (mass) balances and the enthalpy balance must be explicitly accounted for.

Several relevant modeling efforts for CPO without steam (and some also for CPO/ATR with steam) can be found in literature (Hickman and Schmidt, 1993a,b; De Groote and Froment, 1995, 1996; Deutschmann and Schmidt, 1998; Arena et al., 2000; De Smet et al., 2000, 2001), some based on effective rate equations, others on detailed descriptions of transport to the catalyst surface and reactions at the surface. Although several of these models contain some of the elements that are discussed above, we could not find a model that we could confidently use for our objectives.

Based on the above objectives, we set up a reactor model for synthesis gas formation in ATR and CPO processes. Our focus here is on methane, but it is explained how the model can be adapted to multicomponent fuels such as natural gas and naphtha. A one-dimensional (1-D) and stationary (time-independent) model is set up that does not describe mass transfer to the catalyst surface or reaction at the catalyst surface in any detail, but is based on effective rate equations expressed in gas-phase properties (such as Eq. 9) which makes it more straightforward to arrive at a thermodynamically consistent reactor model. For the existing models in literature that contain detailed descriptions of surface reactions in the form of reaction networks, it is only possible to be thermodynamically consistent when enthalpy and entropy of each of the possible surface species are considered, when the enthalpy balance is expanded to include all of these surface species and when each adsorption, surface reaction, and desorption step contains a driving force-term (such as the term within brackets in Eq. 9) based on equilibrium of that specific step (the equilibrium constant in the driving force-term K_i is temperature-dependent, at least for each adsorption and desorption step).

In the model we only consider convective transport of mass and heat in the axial coordinate, which is possible because in CPO and ATR (both autothermal processes, in contrast to steam reforming) heat transfer in a perpendicular direction is negligible (only due to heat loss). Dispersive transport of mass and heat (in axial direction) are also neglected because of the high gas (space) velocities. We use a stationary model because it needs to be practical, and we aim at describing stationary laboratory-scale experiments and using the validated reactor model for design purposes. Instationary aspects are important during startup, shutdown and load-change, but these periods are short in CPO and ATR that operate at a high space velocity.

The model divides the reactor into two subsequent sections. The first (upstream) section is the (partial) oxidation section where all oxygen is converted with part of the fuel and the highest "top" temperature is reached. This section is followed by the reforming section in which the remaining fuel is further converted with water and CO_2 as only possible oxidants to arrive at thermodynamic equilibrium (see Figure 1) (Zhu et al., 2001).

It is well-known that oxygen conversion (in the oxidation section) is very fast. Based on a kinetic analysis, Zhu et al. (2001) estimate the oxidation section to be a few percent of the total reactor, while Kramer et al. (2001) estimate the oxidation section to comprise some 10% of the total reactor volume, based on mass-transfer limited transport in the oxidation section. In the present model we do not assign reactor space to the oxidation section and focus on the reforming section.

At the end of the oxidation section (top), the crude syngas contains all components (CO, CO_2, H_2 and H_2O), as well as part of the fuel, but no oxygen. The fraction of the fuel that is converted in the oxidation section is the "fuel utilization ratio" (UT). A high fuel utilization ratio (for a given amount of air and steam) means that large amounts of CO and H_2 are formed in the oxidation section, resulting in low top temperatures; a low value for UT results in high top temperatures and large amounts of CO_2 and H_2O formed in the oxidation section. In the latter case, more fuel is unconverted in the oxidation section and must be converted in the reforming section. For both reasons, a high value of UT is favorable for CPO/ATR performance. Note that the fuel utilization ratio is equal to one over the oxygen usage ratio in Kramer et al. (2001).

The fuel utilization ratio depends on the relative amounts of air and steam premixed with the fuel, and obviously depends on the rates by which the oxygen and the fuel are transported to the surface, adsorb, and react. When the rate of transport and adsorption of the fuel (methane) is increased (relative to that of oxygen), the fuel utilization ratio increases (Kramer et al., 2001).

The fuel utilization ratio is calculated from the catalyst temperature at the upstream side of the catalyst bed using an optical pyrometer and applying the appropriate mass and enthalpy balances (see Results and Discussion). When deriving the fuel utilization ratio from the measured temperature, it is assumed that, at the end of the oxidation section, the temperatures of gas and catalyst are equal (the "top temperature") and that they coincide with the measured upstream catalyst temperature (see Figure 1). Our experimental observations indicate that this assumption is valid. Such a constant catalyst temperature throughout the oxidation section can be explained when the oxidation reaction is effectively heat- and mass-transfer limited, when (under CPO/ATR conditions) the Chilton-Colburn analogy holds and when the Lewis number (the dimensionless ratio between mass and heat diffusivity) is equal to unity. This case is argued further in Kramer et al. (2001). The assumption that the gas phase has the same temperature as the catalyst at the intersection of the oxidation and reforming section (at the top, see Figure 1) is reasonable given the high heat- and mass-transfer rates, but can also be underpinned by the fact that, in the oxidation section, the gas is colder than the catalyst (the exothermic reactions take place

on the catalyst surface while the gas is heated up by hot molecules coming off the surface), while, in the (endothermic) reforming section, the catalyst should be (somewhat) cooler than the gas. At the intersection of the exothermic and the endothermic regions the temperature of the catalyst and the gas phase should be the same.

In the model it is assumed that the water-gas-shift (WGS) equilibrium is established at each location in the reforming section (thus also at the top where the reforming section starts). That the WGS-equilibrium is established is quite often reported in work on steam reforming and dry reforming (Bodrov et al., 1964; Soliman et al., 1992; Papp et al., 1996; Hou and Hughes, 2001). Also, in experiments with partial fuel conversion (but complete oxygen consumption), we find that the syngas from the reformer is at or close to the WGS-equilibrium. It must be noted that assuming that the WGS-equilibrium is established is not a critical assumption in the current model because of the following reasons: the reaction enthalpy of the WGS-reaction is not very large (small influence on enthalpy balance) and the reaction rate equation that is used for the fuel in the reforming section, as well as the syngas yield-number, are independent of whether the WGS-reaction is at equilibrium or not (for the syngas yield, CO and H_2 are added together).

In the Theory section the model for CPO and ATR is explained in detail for methane as fuel, and for natural gas and naphtha. In the Results and Discussion section, simulation results are presented that are representative of our experience for CPO and ATR of methane.

Theory

Inputs

The two-section model describes the catalytic conversion of methane mixed with air and steam. The inlet molar flows $\phi_{CH4,0}$, $\phi_{air,0}$, $\phi_{water,0}$ [mol/s] are known, as well as the inlet temperature, T_0 [K] and the system pressure, P [Pa] (absolute pressures are used throughout). It is assumed here that the fraction of O_2 in air is χ (namely, $\chi = 0.2095$), and the remainder is N_2, thus $\phi_{O2,0} = \chi \cdot \phi_{air,0}$ and $\phi_{N2,0} = (1 - \chi) \cdot \phi_{air,0}$. The humidity of air is neglected as well as Ar, CO_2, and so on. The oxygen-to-carbon ratio is $\alpha = \phi_{O2,0}/\phi_{CH4,0}$, and the steam-to-carbon ratio is $\gamma = \phi_{H2O,0}/\phi_{CH4,0}$. Simulations are based on a fuel flow of $\phi_{CH4,0} = 10$ mmol/s, which corresponds to 8 kWh (heating value) and ~3 kWe produced in the fuel cell, which is typical of the scale of a single household.

The reactor model consists of a description of the oxidation section in which all oxygen is converted, as well as part of the methane. This conversion is considered to be extremely fast; thus, the catalyst volume required is negligible. The exit of the oxidation section is called the "top" having a certain gas composition and a top temperature. The top is the virtual intersection of the oxidation section and the reforming section. In the model, the entire catalyst volume is assigned to the reforming section.

Heat loss can be implemented in both sections. For the oxidation section, it must be an algebraic expression (as a function of the top temperature, surface area, and so on) or a constant number, Q_{ox} [W]. Heat loss in the reforming section

is a function of the local temperature and is implemented in the (differential) enthalpy balance, Eq. 12.

Simple relations

Some simple relations that will be used without further reference are summarized here. Molar flows ϕ_i [mol/s] are related to the total flow, ϕ_{tot} by $\phi_i = x_i \cdot \phi_{tot}$, with x_i the molar fraction [mol/mol]. Thus, $\phi_{tot} = \sum_i \phi_i$ and $\sum_i x_i = 1$. At the inlet, i runs over max. four species (CH_4, O_2, N_2 and possibly H_2O) and over six species at the top and in the reforming section (CH_4, CO, CO_2, H_2, H_2O and N_2). Partial pressures p_i [Pa] are related to the total pressure P by $\sum_i p_i = P$ and $p_i = x_i \cdot P$.

Thermodynamics

The relevant thermodynamics that is included in the oxidation section and reforming section is summarized in a general form. Enthalpy H_i [J/(mol)] and entropy, S_i [J/(mol·K)] of a certain component i are a function of the local temperature T (see Appendix A).

The two relevant reactions are the water-gas-shift (WGS) reaction

$$CO + H_2O \leftrightarrow CO_2 + H_2$$
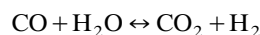
and the methane-steam-reforming (MSR) reaction

$$CH_4 + H_2O \leftrightarrow CO + 3H_2$$
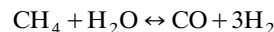
For each reaction, the equilibrium constant K_i is given by

$$K_i = \exp\left(-\frac{1}{RT}\left(\sum_i \nu_i H_i - T \sum_i \nu_i S_i\right)\right) = \prod_i \left(\frac{p_i}{P^*}\right)^{\nu_i} \quad (1)$$

with ν_i the stoichiometric constants in the reaction and $P^* = 101.3$ kPa. For the two reactions the result is

$$K_{WGS} = \exp\left(-\frac{1}{RT}\left((H_{H_2} + H_{CO2} - H_{CO} - H_{H2O})\right.\right.$$
$$\left.\left. - T(S_{H2} + S_{CO2} - S_{CO} - S_{H2O}))\right)\right) =$$
$$= \frac{p_{H2} \cdot p_{CO2}}{p_{H2O} \cdot p_{CO}} = \frac{x_{H2} \cdot x_{CO2}}{x_{H2O} \cdot x_{CO}} = \frac{\phi_{H2} \cdot \phi_{CO2}}{\phi_{H2O} \cdot \phi_{CO}} \quad (2)$$

$$K_{MSR} = \exp\left(-\frac{1}{RT}\left((3 \cdot H_{H2} + H_{CO} - H_{CH4} - H_{H2O})\right.\right.$$
$$\left.\left. - T(3 \cdot S_{H2} + S_{CO} - S_{CH4} - S_{H2O}))\right)\right)$$
$$= \frac{p_{H2}^3 \cdot p_{CO}}{p_{H2O} \cdot p_{CH4}}\left(\frac{1}{P^*}\right)^2 = \frac{x_{H2}^3 \cdot x_{CO}}{x_{H2O} \cdot x_{CH4}}\left(\frac{P}{P^*}\right)^2$$
$$= \frac{\phi_{H2}^3 \cdot \phi_{CO}}{\phi_{H2O} \cdot \phi_{CH4}} \frac{1}{\phi_{tot}^2}\left(\frac{P}{P^*}\right)^2 \quad (3)$$

Atomic balances are based on the fact that at stationary conditions, and for a 1-D reactor model, at each location, the mole flow of each atom (C, H, O, N) is constant (thus equal to the inlet 0 conditions). Thus, at each location j, the balances for C, H, O and N are

$$\phi_{CH4,0} = \phi_{CH4,j} + \phi_{CO,j} + \phi_{CO2,j}$$

$$\phi_{CH4,0} \cdot (4 + 2 \cdot \gamma) = 4 \cdot \phi_{CH4,j} + 2 \cdot (\phi_{H2,j} + \phi_{H20,j})$$

$$\phi_{CH4,0} \cdot (2 \cdot \alpha + \gamma) = \phi_{CO,j} + 2 \cdot \phi_{CO2,j} + \phi_{H2O,j}$$

$$\phi_{N2,0} = \phi_{N2,j} \qquad (4)$$

Oxidation section

In the oxidation section, kinetics are not considered, but a set of algebraic equations describes the conditions at the exit of the oxidation section (the top), which is the intersection with the downstream reforming section. The top temperature T_{top} and the individual gas flows ($\phi_{CH4,top}$, $\phi_{CO,top}$, $\phi_{CO2,top}$, $\phi_{H2,top}$, $\phi_{H2O,top}$, $\phi_{N2,top}$) are unknown. At the end of the oxidation section, oxygen has already vanished. Seven equations are required. We have the WGS-equilibrium, Eq. 2, the four (atomic) mass balances, Eq. 4, and the enthalpy balance

$$\sum_i H_{i,T_0} \cdot \phi_{i,0} = \sum_i H_{i,T_{top}} \cdot \phi_{i,top} + Q_{ox} \qquad (5)$$

with Q_{ox} the heat loss in the oxidation section (W), which can be made an explicit function of T_0, T_{top}, surface area, and so on.

Finally, we introduce the fuel-utilization ratio UT, which describes which part of the fuel is converted in the oxidation section. UT is a function of process conditions, catalyst formulation, and structure. For a specific catalyst, we have derived the empirical function

$$UT = -1.6492 \cdot \alpha^2 + 2.664 \cdot \alpha - 0.2348 - 0.033 \cdot \gamma \qquad (6)$$

from experiments with methane at $T_0 \sim 400°C$ and $P = 170$ kPa in a wide range of values for α and γ (being, respectively, the oxygen-to-carbon and steam-to-carbon ratio). In these experiments the top temperature was measured and the above model was used to derive the appropriate UT-value. Equation 6 is a very accurate description of these data.

Using Eq. 6, $\phi_{CH4,top}$ is given by

$$\phi_{CH4,top} = (1 - UT) \cdot \phi_{CH4,0} \qquad (7)$$

Note that this set of equations does not explicitly describe the selectivities to H_2 and CO (relative to the formation of H_2O and CO_2). However, selectivities can be directly calculated from the oxidation-model (based on Eq. 6, atom and enthalpy balances and the WGS-equilibrium). In general (for a given α and γ), the higher UT, the more selective the oxidation section and the lower the top temperature.

Reforming section

Transport and reaction in the reforming section are described by a plug-flow model. The four atomic balances are used, as well as the enthalpy balance and the WGS-equilibrium. One differential mass balance is required to obtain a 1-D, stationary, plug-flow model for the reforming section. Ideally, this is a mass balance in one of the rate-limiting reactants, typically in the fuel component (but not necessarily so). Indeed, we will use a differential mass balance that describes the conversion of methane. Based on literature (Akers and Camp, 1955; Bodrov et al., 1964; Ridler and Twigg, 1989; Rostrup-Nielsen, 1993; Steghuis et al., 1998) and our own experience, a power law rate equation is proposed for the reforming of methane that is first order in the partial pressure of the fuel component, methane. A first order rate equation in the fuel is compatible with the idea that mass transfer, adsorption or dissociation of the fuel is rate limiting.

At stationary conditions, a differential mass balance over a "slice" in the reforming section results for component i in

$$\frac{d\phi_i}{dz} = R_i \cdot S \qquad (8)$$

with S the cross-sectional surface area [m^2], z the reactor coordinate [m], ϕ_i the mole flow of i [mol/s] and R_i the formation rate of i [mol/(m$^3 \cdot$s)].

For methane conversion, the following effective rate equation is proposed based on a first-order dependence on the partial pressure of methane and an empirical term (in between brackets) that is based on local partial pressures and (via K_{MSR}) on the local temperature, which describes how closely thermodynamic equilibrium has been approached. The result is

$$R_{CH4} = -a \cdot k_0 \cdot e^{-E_A/RT} p_{CH4} \left[1 - \frac{p_{H2}^3 \cdot p_{CO}}{K_{MSR} \cdot p_{CH4} p_{H2O}} \frac{1}{P^{*2}} \right] \qquad (9)$$

in which a is the specific surface area a (m^2 of active phase per m^3 of reactor volume), which is a function of the amount of active phase and details of catalyst preparation, form, and structure; k_0 is the pre-exponential kinetic number, E_A the activation energy [J/mol] of the reaction, and R is the gas constant [J/(mol$\cdot$K)]. The activation energy of reforming reactions is often reported to be in the 100 kJ/mol-range: Hou and Hughes (2001) suggest $E_A = 100$ kJ/mol (based on their Figure 4) and $E_A = 95$ kJ/mol (Figure 12), while Steghuis et al. (1998) measure $E_A = 105$–114 kJ/mol. K_{MSR} is a direct function of the local temperature and is given by the first equality in Eq. 3.

Because the WGS-equilibrium is assumed to be established throughout the reforming section, the driving force term (between brackets) based on the MSR-reaction can be rewritten to a form based on the dry reforming (DR) equilibrium ($CH_4 + CO_2 \leftrightarrow 2 \cdot CO + 2 \cdot H_2$) or to a form based on any of the other possible reactions of methane with water and CO_2. All give exactly the same result.

Equation 9 is implemented in Eq. 8, while partial pressures are recalculated to flows ϕ_i. Furthermore, z and S are replaced by the catalyst volume V [m^3] and a dimensionless reactor coordinate $0 < L^* < 1$, $z \cdot S = L^* \cdot V$. Finally, the group

$a \cdot k_0 \cdot V$ is replaced by λ [mol/(Pa·s)], resulting in

$$\frac{d\phi_{CH4}}{dL^*} = -\lambda e^{-E_A/RT} p_{CH4}\left[1 - \frac{p_{H2}^3 \cdot p_{CO}}{K_{MSR} \cdot p_{CH4} \cdot p_{H2O}}\frac{1}{P^{*2}}\right] \rightarrow$$

$$\frac{d\phi_{CH4}}{dL^*} = -\lambda e^{-E_A/RT} P \phi_{CH4} \phi_{tot}^{-1}$$

$$\times \left[1 - \frac{\phi_{H2}^3 \cdot \phi_{CO}}{K_{MSR} \cdot \phi_{CH4} \cdot \phi_{H2O}}\left(\frac{P}{P^*}\right)^2 \frac{1}{\phi_{tot}^2}\right] \quad (10)$$

Note that Eq. 10 does not directly specify whether methane reacts with water or CO_2, nor does it specify the products; it only describes the conversion rate of methane. However, in conjunction with the WGS-equilibrium and the atom balances (Eqs. 4), the conversion rates of all other components are fixed at each location L^*.

Finally, the differential enthalpy balance is given by

$$\frac{d\sum_i H_i \phi_i}{dz} = -U \cdot P_R \cdot (T - T^*) \quad (11)$$

Here, an engineering heat-transfer relation is used for heat loss through the wall of the reactor. U is an effective heat-transfer coefficient [W/(m²·K)], T^* is a representative temperature outside the reactor, and P_R is the perimeter (m). Multiplying each side by V/S and replacing $U \cdot P_R \cdot V/S$ by κ [W/K] results in

$$\frac{d\sum_i H_i \phi_i}{dL^*} = -\kappa \cdot (T - T^*) \quad (12)$$

At each location, that is, at each L^*-value, the two differential equations (Eqs. 10 and 12), are solved, as well as the four atom balances (Eqs. 4), the WGS-equilibrium (Eq. 2), and the first equality in Eq. 3. Because the temperature T changes as a function of L^*, all terms H_i, S_i, K_{WGS}, and K_{MSR} change with L^*, as well as all ϕ_i's and ϕ_{tot}; P, κ, λ, and T^* are constant throughout.

Coke formation

From separate thermodynamic calculations one can derive the following inequality that predicts below what critical temperature, $T_{critical}$ [K], coke formation is thermodynamically expected

$$T_{critical} = 3.1368 \cdot (\ln(A))^2 - 45.791 \ln(A) + 973.51$$

$$\text{with } A = \frac{p_{CO2}}{p_{CO}^2}P^* = \frac{x_{CO2}}{x_{CO}^2}\frac{P^*}{P} = \frac{\phi_{CO2}}{\phi_{CO}^2}\phi_{tot}\frac{P^*}{P} \quad (13)$$

After having determined the thermodynamic equilibrium gas-phase composition assuming zero coke formation, Eq. 13 can be used to check whether that assumption was correct. Coke formation is not predicted in the relevant cases for ATR/CPO we considered, with the equilibrium temperature of the synthesis gas typically ~ 100 K above that required for coke formation. This is in alignment with our experiments in which coke formation in the reactor is not observed under normal operating conditions.

Natural gas

The model for ATR/CPO of methane can be extended to describe the conversion of natural gas—if methane makes up the majority of the hydrocarbons in the natural gas, which is generally the case. The two-section model for methane can be used as long as we assume that all hydrocarbons except for CH_4 are consumed in the oxidation step (Akers and Camp, 1955). The parameters α and γ required in Eq. 6 are best defined relative to the total inlet hydrocarbon flow, $\phi_{C,0}$: $\alpha = \phi_{O2,0}/\phi_{C,0}$ and $\gamma = \phi_{H2O,0}/\phi_{C,0}$ with $\phi_{C,0}$ given by a summation over all hydrocarbons

$$\phi_{C,0} = \sum_i C_i \cdot \phi_{C_i,0} \quad (14)$$

with C_i the C-number of component i (such as $C = 2$ for C_2H_6). Further, Eq. 7 must be replaced by

$$\phi_{CH4,top} = (1 - UT) \cdot \phi_{C,0} \quad (15)$$

Naphtha and other multicomponent fuels

Naphtha is a complex mixture of components mainly in the $C_5 - C_{12}$ range. Instead of dealing with each component separately, it is possible to simplify the analysis by proper averaging. For example, a fuel mixture of 25 mol. % toluene, 25% methylcyclohexane, 25% n-heptane, and 25% iso-octane can be summarized by the formula $C_{7.25}H_{14}$ with the enthalpy function $H = -6 \cdot 10^{-5} \cdot T^3 + 0.2638 \cdot T^2 + 15.249 \cdot T - 153627$ [J/mol] correct within $\sim 1\%$ in the relevant temperature range $298 < T$ [K] $< 1,400$.

A reformer model for naphtha can be derived from the methane two-section model. For the oxidation section, a utilization-function for naphtha must be used which is not necessarily the same as Eq. 6, as well as an additional equation for the formation of methane and other hydrocarbons (although methane is the most relevant one; the formation rates of higher hydrocarbons are negligible with ppm- or ppb-levels in the equilibrium mixture). Methane formation in the oxidation section can be set to zero, $\phi_{CH4,top} = 0$, or an equilibrium can be used, such as the MSR-equilibrium or the dry reforming equilibrium (DR).

In the reforming section a differential mass balance for naphtha conversion (such as first order in naphtha) replaces Eq. 10. A driving force-term, such as used in Eq. 10 is not required, as, at thermodynamic equilibrium, naphtha-conversion is complete. For methane formation, the MSR- or DR-equilibrium can be used or a reaction rate equation, such as based on the methanation mechanism (with the rate dependent on the partial pressures of CO and H_2). We find that the DR-equilibrium is in many cases established (at the exit of the reactor) and use the DR-equilibrium in the reforming section.

Results and Discussion

In the first part of Results and Discussion, experimental results of the conversion of methane in ATR/CPO are compared with predictions of the two-section model. In the second part somewhat other parameter settings are used and simulation results are presented for top temperature and methane conversion behavior.

Two remarks must be made with respect to methane conversion ζ and utilization UT. First, whereas ζ is the "actual" conversion measured at the end of the reactor, thus at the end of the reforming section, the fuel utilization ratio UT is actually equal to the methane conversion at the end of the oxidation section $(0 < UT < 1)$. The difference between UT and ζ is a measure of the fuel conversion in the reforming section.

Second, in CPO/ATR of methane, the methane conversion ζ is directly related to the syngas yield Y (mole flow of produced $CO + H_2$ divided by the mole flow of CH_4 fed to the reactor). This relation follows from a combination of the atom balances for C, H, and O, and is given by

$$Y = 4 \cdot \zeta - 2 \cdot \alpha \qquad (16)$$

in which ζ is the methane conversion $(0 < \zeta < 1)$ and α is the (molecular) oxygen-to-carbon ratio. Thus, methane conversion results can be recalculated directly to syngas yield numbers. Equation 16 can be used to calculate the actual syngas yield (based on ζ), the syngas yield after the oxidation section (based on UT), and the maximum attainable syngas yield (based on the conversion at thermodynamic equilibrium).

Comparison of two-section model with experimental results

Experimental data for top temperature and methane conversion are presented for a system pressure of 170 kPa and an inlet temperature of $T_0 \sim 400°C$ in Figure 3 and Figure 4 for different values of the oxygen-to-carbon ratio α, and the steam-to-carbon ratio γ. Each experiment is analyzed individually and a different heat loss is calculated for each experiment by the difference of the total enthalpy leaving and entering the reactor (inlet temperature measured using a thermocouple; exit temperature by assuming the WGS-equilibrium; exit composition based on GC-analysis). In the analysis the heat loss is completely assigned to the oxidation section; therefore, Q_{ox} of Eq. 5 can be measured. In the analysis of the data (Figures 3 and 4) heat loss in the reforming section is set to zero (κ in Eq. 12 set to zero). Due to the fact that the heat loss is different for each experiment, the lines for top temperature (Figure 3), conversion, and thermodynamic equilibrium (Figure 4) are somewhat jagged. The heat loss was in all cases small compared to the total energy content (in combustion) of the entire gas flow.

From each experimental value of top temperature (symbols in Figure 3), the utilization of methane (UT) can be calculated (circles in Figure 4) using the oxidation model that is based on atom balances, the enthalpy balance, and the WGS-equilibrium (that is, given these constraints, only for one value of UT is the measured top temperature, at the exit of the oxidation section, obtained). The top temperature decreases when the amount of air is reduced or the amount of

steam is increased. The empirical utilization function (Eq. 6) describes these data quite well (see the lower solid lines in Figure 4). Using Eq. 6 and the other elements of the oxidation model, the top temperature can be back-calculated. The result is plotted as the solid lines in Figure 3. For the highest oxygen-to-carbon ratio $\alpha = 0.59$, the prediction is accurate; for the two lower oxygen-to-carbon ratios, the prediction is less accurate but is certainly showing the right trends.

The data for methane conversion, ζ (squares) are presented in Figure 4 together with the predicted conversion at thermodynamic equilibrium (upper solid lines). By adjusting λ and E_A (given a suitable form of the rate equation (Eq. 10), the two-section reactor model (dashed lines) can be fitted to the methane conversion data.

For each oxygen-to-carbon ratio α, the difference between the utilization UT and the actual conversion ζ (the difference representing the conversion in the reforming section) first increases with γ (starting from $\gamma = 0$), but above a certain γ-value (0.5−0.75) becomes constant: UT and ζ decrease simultaneously as if the conversion in the reforming section becomes independent of γ. The constant difference of ζ and UT increases with α, namely from ζ-$UT = 0.17$ at $\alpha = 0.42$ to 0.20 at $\alpha = 0.52$ and 0.23 at $\alpha = 0.59$. Although the gap between UT and ζ remains fairly constant for a given α and for enough steam (above $\gamma \sim 0.5-0.75$), the gap between UT and the thermodynamically attainable conversion increases with increasing amounts of steam, γ.

For each value of α ($\alpha = 0.42$ in Figure 4a, $\alpha = 0.52$ in Figure 4b, and $\alpha = 0.59$ in Figure 4c), thermodynamic equilibrium conversion (upper solid line) was reached at the end of the reforming section for zero steam addition $\gamma = 0$. With increasing amounts of steam, the actual conversion ζ first increases, then levels off and finally starts to decrease. This occurs while the thermodynamically attainable conversion continuously increases with γ. As a consequence, the gap between the actual conversion ζ and that what is thermodynamically attainable increases with γ. Interestingly, the gap between the actual conversion ζ and thermodynamic equilib-
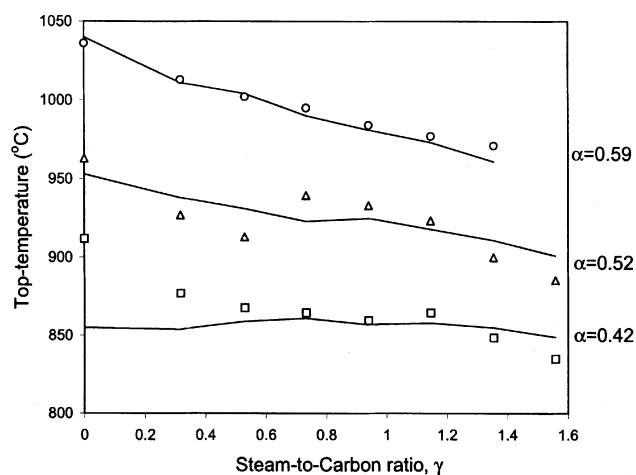

Figure 3. Top temperature in ATR/CPO of methane.

Different steam-to-carbon ratios γ and oxygen-to-carbon ratios α. $T_0 \sim 400°C$, $P = 150$ kPa, varying heat loss. Lines are predictions of the oxidation model.

rium is about the same for each value of the oxygen-to-carbon ratio α, although both values strongly increase with α.

That thermodynamic equilibrium is only reached at low to zero steam loads and is due to the decreasing utilization in the oxidation section and the lower reaction rates in the reforming section when α is increased. The lower reaction rate is due to the lower temperatures throughout the reforming section, and the higher total gas-flow rate ϕ_{tot}, resulting in a lower methane partial pressure. Both effects are due to the presence of the additional steam. Thus, the thermodynamic advantage of adding more steam (if available at a low cost at T_0) can only be attained with more catalyst (or at a lower space velocity).

As discussed, the gap between the actual observed conversion, and the potential, thermodynamically attainable, conversion does not depend much on the oxygen-to-carbon ratio α. This shows that several opposing mechanisms occur simul-

taneously: although reactor temperatures are much higher at the high air-load (high value for α), the methane partial pressure is decreased due to the additional nitrogen, while the actual conversion required in the reforming section (to keep the gap constant) increases with α (from ~ 0.17 at $\alpha = 0.42$ to ~ 0.23 at $\alpha = 59$).

Further simulations

For other parameter settings, simulation results are presented in Figures 5–7. Figure 5 focuses on the oxidation section and shows the top temperature and methane utilization as a function of the oxygen-to-carbon ratio α. The top temperature is plotted on the lefthand y-axis and increases with more oxygen and less steam. The utilization is plotted on the righthand y-axis (dashed lines) and, as in Figure 4, increases with more oxygen and less steam. Again, as in Figure 4, the
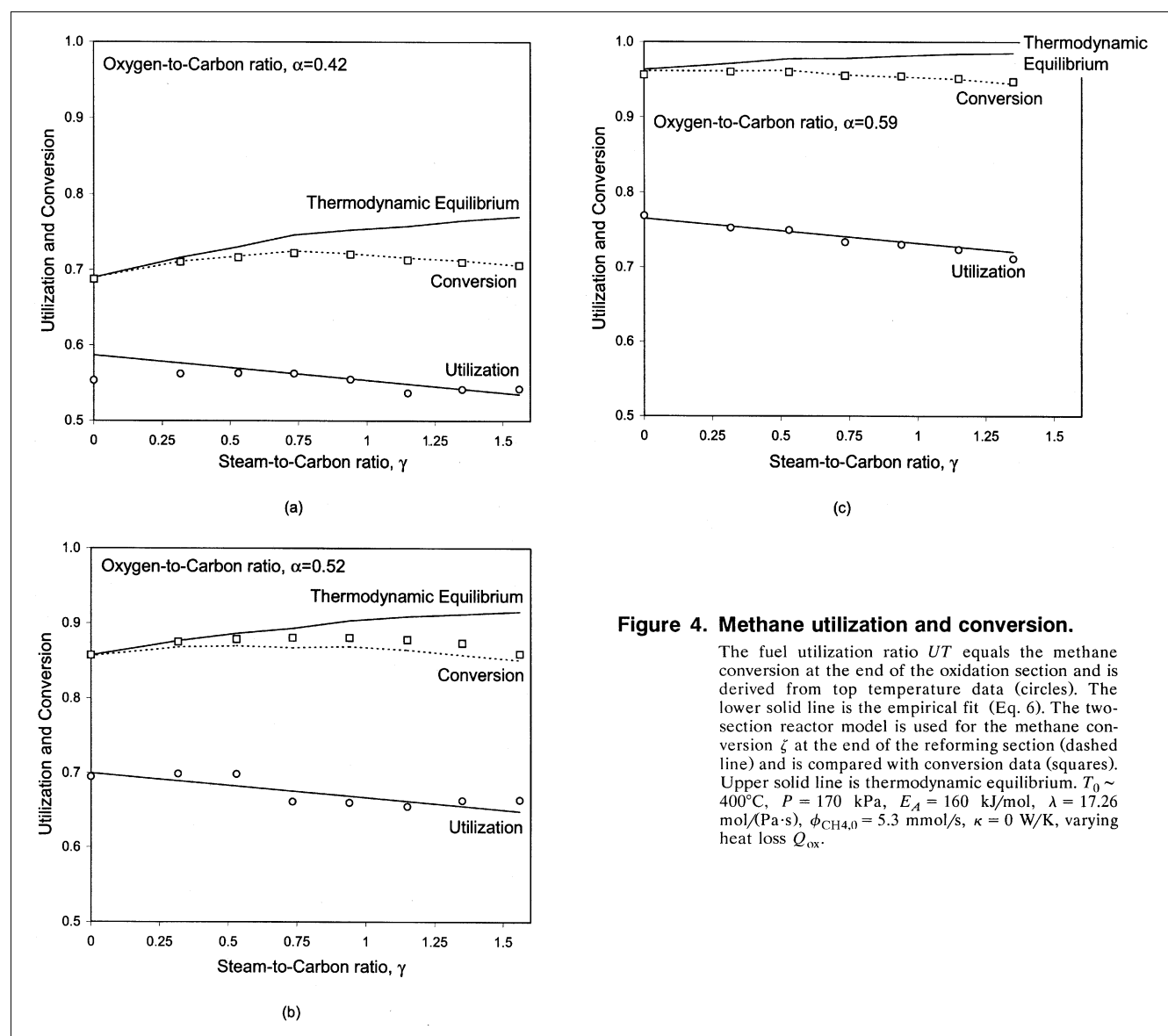

Figure 4. Methane utilization and conversion.

The fuel utilization ratio UT equals the methane conversion at the end of the oxidation section and is derived from top temperature data (circles). The lower solid line is the empirical fit (Eq. 6). The two-section reactor model is used for the methane conversion ζ at the end of the reforming section (dashed line) and is compared with conversion data (squares). Upper solid line is thermodynamic equilibrium. $T_0 \sim 400°C$, $P = 170$ kPa, $E_A = 160$ kJ/mol, $\lambda = 17.26$ mol/(Pa·s), $\phi_{CH4,0} = 5.3$ mmol/s, $\kappa = 0$ W/K, varying heat loss Q_{ox}.
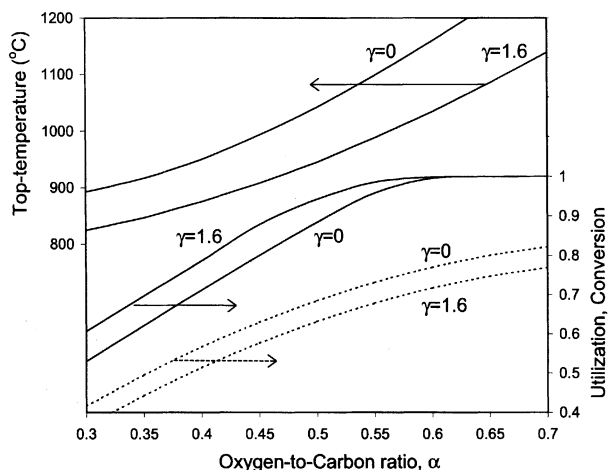
Figure 5. Oxidation Section in ATR/CPO of methane.

Variation of oxygen-to-carbon ratio α and steam-to-carbon ratio γ. Top temperature on left y-axis. Thermodynamic conversion (solid lines on right y-axis), as well as the fuel utilization (dashed lines). $T_0 = 400°C$, $Q_{ox} = 0$ W, $P = 150$ kPa.

maximum, thermodynamically attainable, conversion (solid lines) increases with more steam and oxygen. For the pressure of 150 kPa, only for sufficient amounts of oxygen (in this case, for $\alpha > 0.6$) is the thermodynamic methane conversion close to 100%. For a lower α, the thermodynamic, maximum, fuel conversion is significantly reduced and most significantly without steam ($\gamma = 0$).

Figure 5 indicates once more that, with more steam, the utilization (conversion in oxidation section) decreases while the attainable (maximum) conversion increases: more fuel must be converted in the reforming section.

Simulation results of the development of temperature and methane conversion through the reforming section are presented in Figure 6. Methane conversion is directly coupled to syngas yield using Eq. 16. The top temperature is higher without steam, which is one reason why conversion is already complete at $L^* \sim 0.3$. For $\gamma = 1.6$, methane is converted along the entire reactor coordinate, with thermodynamic equilibrium not yet reached at $L^* = 1$.

Comparing $\gamma = 0$ and $\gamma = 1.6$ shows that, for $\gamma = 1.6$, more catalyst is required to arrive at thermodynamic equilibrium, but that the methane conversion and syngas yield associated with equilibrium are higher ($+1.5\%$ and $+1\%$, respectively) than at zero steam load.

In case of heat loss through the reactor wall $\kappa > 0$, the situation becomes more complicated, and it is possible that, for a low γ, resulting in fast reactions and low catalyst volumes, the optimum L^* corresponds to a higher methane conversion (thus, a higher syngas yield). Figure 7 shows that, for $\gamma = 0$, the maximum methane conversion is found at $L^* \sim 0.14$ and is 95.7%, whereas, for $\gamma = 1.6$, the maximum methane conversion is 91.5% at $L^* \sim 0.63$. This behavior is opposite to what is predicted for thermodynamic equilibrium and without heat loss, in which case methane conversion is higher for $\gamma = 1.6$ than for $\gamma = 0$ (see Figure 6). In the decreasing portions of the conversion curves (Figure 7) thermodynamic equilibrium has already been rather well-estab-
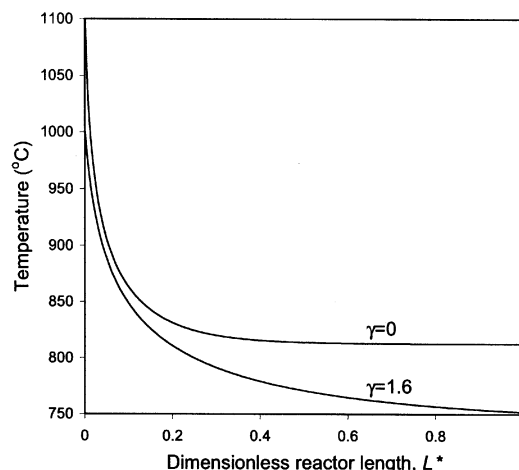
(a)
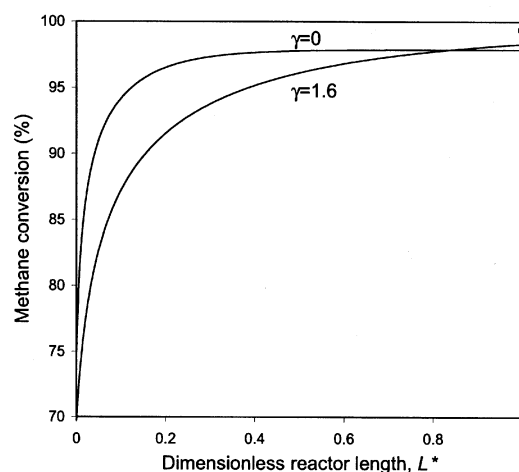
(b)

Figure 6. Temperature profile (a) and methane conversion (b) as a function of reactor coordinate L^* for two steam-to-carbon ratios γ.

The circle shows the equilibrium value for $\gamma = 1.6$ ($\alpha = 0.57$, $P = 150$ kPa, $\phi_{CH4,0} = 10$ mmol/s, $T_0 = 400°C$, $\lambda = 0.10$ mol/(Pa·s), $E_A = 100$ kJ/mol, $Q_{ox} = 0$ W, $\kappa = 0$ W/K).

lished, but due to heat loss, the temperature decreases and methane is formed again (methanation).

Conclusions

A two-section reactor model describes several key features of fuel conversion in autothermal reforming (CPO and ATR) based on air and steam, such as the high upstream temperature, as well as the decreasing temperature throughout the reforming section. The model can be fitted to data to obtain an optimum value for the kinetic constant, activation energy, and reaction order. For a given amount of catalyst and with increasing steam loads, the temperature in the reactor decreases, and the methane conversion (and yield of hydrogen and CO) first increases and then decreases, while the conversion that is thermodynamically feasible continuously in-
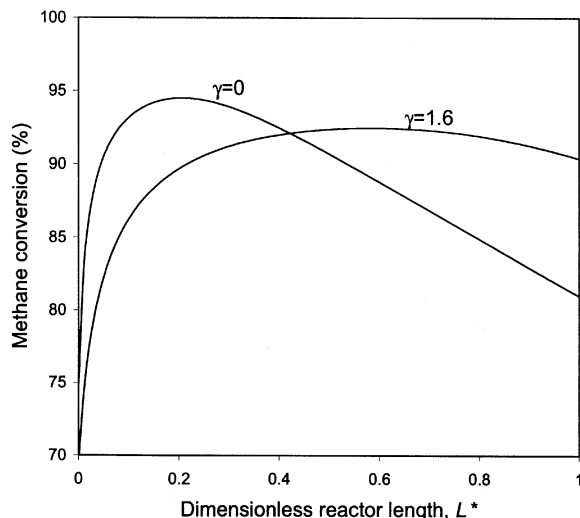
Figure 7. Methane conversion with heat loss in the reforming section, as function of γ and L^*.

$\kappa = 1$ W/K, $T^* = 298.15$ K, all other data see Figure 6.

creases. Thus, the thermodynamic advantage of adding more steam can only be attained at a lower space velocity. The model can be extended to describe multicomponent fuels such as natural gas and naphtha.

Acknowledgments

Notation

a = specific surface area of catalyst, m²/m³
c_i = concentration of component, i, mol/m³
E_A = activation energy of reaction i, J/mol
H_i = enthalpy of component i, J/mol
k_0 = pre-exponential kinetic number, mol/(m²·Pa·s)
K_i = equilibrium constant of reaction i (either WGS or MSR)
L^* = dimensionless axial reactor coordinate
p_i = partial pressure of component i, Pa
P = absolute pressure, Pa
P^* = reference pressure = $1.013·10^5$ Pa
P_R = perimeter of the reactor, m
Q_{ox} = heat loss in oxidation section, W
R = gas constant = 8.3144 J/(mol·K)
R_i = reaction rate of reaction i, mol/(m³·s)
S = cross-sectional surface area of reactor, m²
S_i = entropy of component i, J/(mol·K)
t = time, s
T = temperature, K
T_0 = inlet temperature, K
T^* = temperature outside of reactor, K
UT = fuel utilization ratio
U = effective heat transfer coefficient, W/(m²·K)
V = reactor volume, m³
x_i = mole fraction of component i, mol/mol
z = reactor coordinate in axial direction, m

Greek letters

α = oxygen-to-carbon ratio of inlet flow (= $\phi_{O2,0}/\phi_{CH4,0}$)
γ = steam-to-carbon ratio of inlet flow (= $\phi_{H2O,0}/\phi_{CH4,0}$)
ζ = methane conversion (at the end of reforming section)
κ = $U·P_R·V/S$, W/K
λ = $a·k_0·V$, mol/(Pa·s)
ν_i = stoichiometric constant of reactant i
ϕ_i = mole flows of component i, mol/s
$\phi_{i,0}$ = inlet mole flows of component i, mol/s
ϕ_{tot} = total mole flow, mol/s
$\phi_{i,top}$ = mole flow of component i at the intersection of oxidation and reforming section, mol/s
χ = fraction of oxygen in air (= 0.2095)

Literature Cited

Ahmed, S., and M. Krumpelt, "Hydrogen from Hydrocarbon Fuels for Fuel Cells," *Int. J. Hydrogen Energy*, **26**, 291 (2001).

Akers, W. W., and D. P. Camp, "Kinetics of the Methane-Steam Reaction," *AIChE J.*, **1**, 471 (1955).

Arena, F., F. Frusteri, and A. Parmaliana, "Kinetics of the Partial Oxidation of Methane to Formaldehyde on Silica Catalyst," *AIChE J.*, **46**, 2285 (2000).

Bodke, A. S., S. S. Bharadwaj, and L. D. Schmidt, "The Effect of Ceramic Supports on Partial Oxidation of Hydrocarbons over Noble Metal Coated Monoliths," *J. Catalysis*, **179**, 138 (1998).

Bodrov, N. M., L. O. Apel'baum, and M. I. Temkin, "Kinetics of the Reaction of Methane with Steam on the Surface of Nickel," *Kinet. Catal.*, **5**, 614 (1964).

Chang, Y.-F., and H. Heinemann, "Partial Oxidation of Methane to Syngas over Co/MgO Catalysts. Is it Low Temperature?," *Catalysis Letters*, **21**, 215 (1993).

Daubert, T. E., and R. P. Danner, *Data Compilation Tables of Properties of Pure Compounds*, AIChE, New York (1985).

De Groote, A., and G. F. Froment, "Reactor Modeling and Simulations in Synthesis Gas Production," *Reviews in Chem. Eng.*, **11**, 145 (1995).

De Groote, A., and G. F. Froment, "Simulation of the Catalytic Partial Oxidation of Methane to Synthesis Gas," *Applied Catalysis A: General*, **138**, 245 (1996).

De Smet, C. R. H., M. H. J. M. de Croon, R. J. Berger, G. B. Marin, and J. C. Schouten, "Kinetics for the Partial Oxidation of Methane on a Pt Gauze at Low Conversions," *AIChE J.*, **46**, 1837 (2000).

De Smet, C. R. H., M. H. J. M. de Croon, R. J. Berger, G. B. Marin, and J. C. Schouten, "Design of Adiabatic Fixed Bed Reactors for the Partial Oxidation of Methane to Synthesis Gas. Application to Production of Methanol and Hydrogen-for-Fuel-Cells," *Chem. Eng. Sci.*, **56**, 4849 (2001).

Deutschmann, O., and L. D. Schmidt, "Modeling the Partial Oxidation of Methane in a Short-Contact-Time Reactor," *AIChE J.*, **44**, 2465 (1998).

Dissanayake, D., M. P. Rosynek, K. C. C. Kharas, and J. H. Lunsford, "Partial Oxidation of Methane to Carbon Monoxide and Hydrogen over a Ni/Al$_2$O$_3$ Catalyst," *J. Catalysis*, **132**, 117 (1991).

Docter, A., and A. Lamm, "Gasoline Fuel Cell Systems," *J. Power Sources*, **84**, 194 (1999).

Elvers, B., et al., ed., *Ullmann's Encyclopedia of Industrial Chemistry*, Volume A12, p. 207, 5th Ed., VCH, Weinheim (1989).

Heitnes Hofstad, K., T. Sperle, O. A. Rokstad, and A. Holmen, "Partial Oxidation of Methane to Synthesis Gas over a Pt/10% Rh Gauze," *Catalysis Letters*, **45**, 97 (1997).

Hickman, D. A., and L. D. Schmidt, "Production of Syngas by Direct Catalytic Oxidation of Methane," *Science*, **259**, 343 (1993a).

Hickman, D. A., and L. D. Schmidt, "Steps in CH$_4$ Oxidation on Pt and Rh Surfaces: High Temperature Reactor Simulations," *AIChE J.*, **39**, 1164 (1993b).

Hou, K., and R. Hughes, "The Kinetics of Methane Steam Reforming over a Ni/α-Al$_2$O Catalyst," *Chem. Eng. J.*, **82**, 311 (2001).

Kramer, G. J., W. Wieldraaijer, P. M. Biesheuvel, and H. P. C. E. Kuipers, "The Determining Factor for Catalyst Selectivity in Shell's Catalytic Partial Oxidation Process," *ACS Fuel Chemistry Division Preprints*, **46**, 659 (2001).

Table A1. Thermodynamic Data

	$H_{0,i}$ (kJ/mol)	$S_{0,i}$ (J/mol/K)	a_i (J/mol/K)	b_i (J/mol/K)	c_i (K)	d_i (J/mol/K)	e_i (K)
CH_4	-74.5	186.27	33.298	79.933	2,086.9	41.602	991.96
O_2	0	205.04	29.103	10.04	2,526.5	9.356	1,153.8
CO	-111	197.54	29.108	8.773	3,085.1	8.4553	1,538.2
CO_2	-394	213.69	29.37	34.54	$-1,428$	26.4	588
H_2	0	130.57	27.617	9.56	2,466	3.76	567.6
H_2O	-242	188.72	33.363	26.79	2,610.5	8.896	1169
N_2	0	191.609	29.105	8.6149	1,701.6	0.10347	909.79

Moon, D. J., K. Sreekumar, S. D. Lee, B. G. Lee, and H. S. Kim, "Studies on Gasoline Fuel Processor System for Fuel-Cell Powered Vehicles Application," *Applied Catalysis A: General*, **215**, 1 (2001).

Papp, H., P. Schuler, and Q. Zhuang, "CO_2 Reforming and Partial Oxidation of Methane," *Topics in Catalysis*, **3**, 299 (1996).

Prettre, M., Ch. Eichner, and M. Perrin, "The Catalytic Oxidation of Methane to Carbon Monoxide and Hydrogen," *Trans. Faraday Soc.*, **43**, 335 (1946).

Ridler, D. E., and M. V. Twigg, "Steam Reforming," Ch. 5 in *Catalyst Handbook*, M. V. Twigg, ed., Manson Publishing, London (1989).

Rostrup-Nielsen, J. R., "Production of Synthesis Gas," *Catalysis Today*, **18**, 305 (1993).

Service, R. F., "Bringing Fuel Cells Down to Earth," *Science*, **285**, 682 (1999).

Soliman, M. A., A. M. Adris, A. S. Al-Ubaid, and S. S. E. H. El-Nashaie, "Intrinsic Kinetics of Nickel/Calcium Aluminate Catalyst for Methane Steam Reforming," *J. Chem. Tech. Biotechnol.*, **55**, 131 (1992).

Steghuis, A. G., J. G. van Ommen, and J. A. Lercher, "On the Reaction Mechanism for Methane Partial Oxidation over Yttria/Zirconia," *Catalysis Today*, **46**, 91 (1998).

Wang, H. Y., and E. Ruckenstein, "Catalytic Partial Oxidation of Methane to Synthesis Gas over γAl_2O_3-Supported Rhodium Catalysts," *Catalysis Lett.*, **59**, 121 (1999).

Zhu, J., D. Zhang, and K. D. King, "Reforming of CH_4 by Partial Oxidation: Thermodynamic and Kinetic Analyses" *Fuel*, **80**, 899 (2001).

Appendix A

Enthalpy H_i and entropy S_i are expressed as (Daubert and Danner, 1985)

$$H_i = H_{0,i} + a_i(T - T_0) + b_i c_i\left(\coth\frac{c_i}{T} - \coth\frac{c_i}{T_0}\right)$$
$$- d_i e_i\left(\tanh\frac{e_i}{T} - \tanh\frac{e_i}{T_0}\right)$$

$$S_i = S_{0,i} + a_i \ln\frac{T}{T_0} + b_i\left(\frac{c_i}{T}\coth\frac{c_i}{T} - \frac{c_i}{T_0}\coth\frac{c_i}{T_0} - \ln\frac{\sinh\left(\frac{c_i}{T}\right)}{\sinh\left(\frac{c_i}{T_0}\right)}\right)$$
$$- d_i\left(\frac{e_i}{T}\tanh\frac{e_i}{T} - \frac{e_i}{T_0}\tanh\frac{e_i}{T_0} - \ln\frac{\cosh\left(\frac{e_i}{T}\right)}{\cosh\left(\frac{e_i}{T_0}\right)}\right)$$

with $T_0 = 298.15$ K and $\coth = 1/\tanh$. The values for $a_i - e_i$ are summarized in Table A1.